Bistability in the redox chemistry of sediments and oceans

Sebastiaan J. van de Velde[a,1], Christopher T. Reinhard[b], Andy Ridgwell[a], and Filip J. R. Meysman[c,d,1]

[a]Department of Earth and Planetary Sciences, University of California, Riverside, CA 92521; [b]School of Earth and Atmospheric Sciences, Georgia Institute of Technology, Atlanta, GA 30332; [c]Department of Biology, University of Antwerp, 2160 Wilrijk, Belgium; and [d]Department of Biotechnology, Delft University of Technology, 2629 HZ Delft, The Netherlands

Edited by James Farquhar, University of Maryland, College Park, MD, and approved November 17, 2020 (received for review April 27, 2020)

For most of Earth's history, the ocean's interior was pervasively anoxic and showed occasional shifts in ocean redox chemistry between iron-buffered and sulfide-buffered states. These redox transitions are most often explained by large changes in external inputs, such as a strongly altered delivery of iron and sulfate to the ocean, or major shifts in marine productivity. Here, we propose that redox shifts can also arise from small perturbations that are amplified by nonlinear positive feedbacks within the internal iron and sulfur cycling of the ocean. Combining observational evidence with biogeochemical modeling, we show that both sedimentary and aquatic systems display intrinsic iron–sulfur bistability, which is tightly linked to the formation of reduced iron–sulfide minerals. The possibility of tipping points in the redox state of sediments and oceans, which allow large and nonreversible geochemical shifts to arise from relatively small changes in organic carbon input, has important implications for the interpretation of the geological rock record and the causes and consequences of major evolutionary transitions in the history of Earth's biosphere.

redox cycling | bistability | alternative stable states | sediments

The modern oceans are pervasively oxygenated, with anoxia being restricted to oxygen minimum zones and a few poorly ventilated basins such as the Black Sea (1). In contrast, during the Precambrian and early Phanerozoic Eon, the ocean interior is thought to have been pervasively anoxic (Fig. 1). Reconstruction of the redox evolution of the deep ocean is challenging prior to the Cretaceous due to a lack of rock records that can be unambiguously attributed to deposition in deep-sea environments. Still, redox reconstructions of intermediate water depths are available from a number of localities in the Precambrian and early Phanerozoic Eon, and these data suggest that oceanic basins—or at least subbasins—have alternated spatially and temporally between predominant iron-rich (ferruginous) and sulfide-rich (euxinic) conditions (2–9) (Fig. 1*B*). Recent evidence also suggests that periodic basin-scale transitions between ferruginous and euxinic conditions occurred during the "oceanic anoxic events" during the predominantly oxygenated Mesozoic (10, 11) (Fig. 1*B*). These two contrasting redox states imply a very different chemical environment for marine life, as any shift between them also entails a critical change in the concentrations of limiting elements (such as phosphorus, iron, and molybdenum) that sustain marine productivity and energy flow through the ocean biosphere (12–15).

Transitions between ferruginous and euxinic states on a basin-to-global scale require a switch in the dominant redox chemistry. One mechanism to achieve this is via a shift in the relative rates at which iron and sulfate are delivered to the ocean, with higher iron inputs favoring the prevalence of ferruginous conditions (16, 17). As a result, observed shifts in the redox state of the ocean interior are interpreted as reflecting major state changes in the Earth system, such as an increase in atmospheric oxygen (16), periods with strongly elevated volcanism (2), sea-level changes that modify the extent of the global depositional shelf area (9), or intervals of enhanced Fe or S weathering due to continental breakup (3, 18). An alternative mechanism is that changes in nutrient supply and nutrient availability in the ocean can increase the export of organic matter from the surface to the subsurface ocean. More organic carbon export then leads to increased microbial respiration, stimulating the production of sulfide via sulfate reduction and essentially titrating ferrous iron from the water column as pyrite (18). As a result, switches between ferruginous and euxinic states have been linked to the relative supply or production of ferrous iron and free sulfide, causing transitions at the Fe:S ratio of 1:2, the stoichiometric ratio of pyrite (17, 19).

Here, we present a theoretical analysis of redox shifts in anoxic biogeochemical systems of both the ocean interior and marine sediments. Both these systems display aqueous chemistries that can switch between ferrous-iron–dominated and free-sulfide–dominated states. In this analysis, we focus on the question of whether large shifts in the redox state also necessarily require large perturbations to boundary conditions.

Paleoredox reconstructions often adopt an implicitly linear perspective in their interpretation of the rock record, whereby small changes in external inputs will only cause small shifts, while large shifts in redox chemistry—such as switches between ferruginous and euxinic deep waters—necessitate major changes in external inputs. Here, in contrast, we demonstrate not only that natural anoxic systems may be subject to critical thresholds—so-called "tipping points"—but that alternative stable states exist

Significance

Changes in ocean redox chemistry are frequently observed in Earth's history and have fundamental implications for the evolution of marine life. These transitions are commonly ascribed to large changes in the supply of iron, sulfur, or organic carbon in the deeper ocean. We propose that small variations in carbon input flux can drive nonreversible redox changes of the ocean interior and other anoxic systems, such as marine sediments. Nonlinear interactions in the iron and sulfur cycles create tipping points where regime shifts can occur between alternative stable states that are either iron dominated or sulfide dominated. The recognition that the biogeochemistry of sediments and oceans embeds intrinsic bistability provides a conceptual framework for understanding past and present anoxic marine systems.

Author contributions: F.J.R.M. designed research; S.J.v.d.V. and F.J.R.M. performed research; S.J.v.d.V. and F.J.R.M. analyzed data; S.J.v.d.V., C.T.R., A.R., and F.J.R.M. wrote the paper; and C.T.R. compiled literature data.

The authors declare no competing interest.

This article is a PNAS Direct Submission.

[1]To whom correspondence may be addressed. Email: sebastiaan.van.de.velde@ulb.ac.be or F.J.R.Meysman@tudelft.nl.

This article contains supporting information online at https://www.pnas.org/lookup/suppl/doi:10.1073/pnas.2008235117/-/DCSupplemental.

First published December 14, 2020.

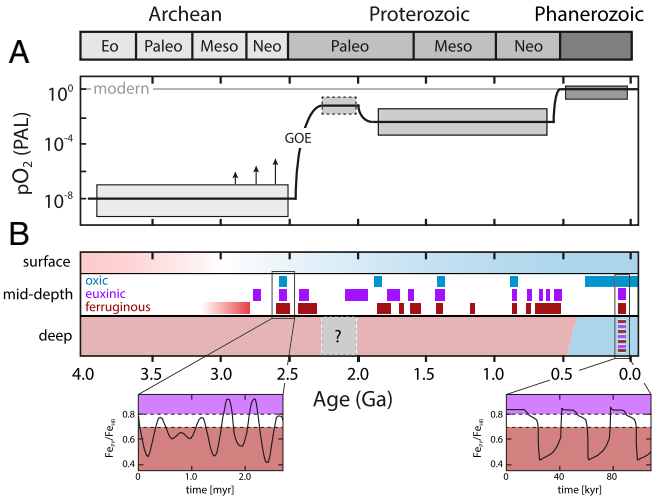

Fig. 1. The evolving redox chemistry of the oceans against the backdrop of atmospheric oxygenation. (*A*) The estimates of the partial pressure of atmospheric oxygen (pO_2) relative to the PAL (43). The upward arrows during the Archaean denote possible transient episodes of ocean-atmosphere oxygenation just prior to the "Great Oxidation Event" (GOE). (*B*) The first-order features of evolving redox in surface, middepth, and deep ocean. The pattern of surface ocean oxygenation displayed is based on isotopic data (44, 45) and equilibration with atmospheric pO_2. Note, however, that surface ocean oxygenation was likely spatially variable (46). The records for intermediate (middepth) settings are after ref. 7, supplemented with observations from refs. 2, 4–6, 8, 10. The insets in *B* schematically depict reported oscillations between ferruginous and sulfidic conditions during the late Archean (47) (*Left*) and during the Cretaceous Thermal Maximum (11) (*Right*). The redox conditions in the deep ocean are tentative. Although a "background" state of ferruginous conditions for the deep ocean is consistent with available data from the sedimentary record, existing empirical constraints are not of sufficiently high fidelity to rule out pervasively euxinic deposition in the deep ocean for certain periods during the Precambrian. The question mark denotes the uncertain (potentially oxic) deep ocean redox state during the Lomagundi interval.

with a hysteresis barrier to reversibility. Our analysis reveals that the redox chemistry of anoxic systems shows nonlinear dynamics, characterized by both strong resilience (large changes in the supply of iron oxides or organic carbon must not necessarily induce a shift in redox chemistry) as well as dramatic shifts near the tipping points. As a result, large and abrupt redox changes may occur in response to small and gradual changes in external forcing, without any significant change in Fe or S input fluxes. The existence of redox tipping points in the ocean interior could have important implications for the interpretation of Earth's evolution.

Results and Discussion

In this study, we systematically examine a series of models that describe the iron and sulfur cycling in different marine environments (both sediments and water column). Drawing upon recent geochemical observations, we first describe that iron and sulfur cycling in modern salt marsh sediments displays a built-in redox dichotomy, where both an iron-rich and sulfide-rich state can occur under identical boundary conditions. Subsequently, we demonstrate that such bistable redox states are not limited to salt marsh sediments but are an inherent feature of models that describe a wider range of natural anoxic sediments. In the third step, we demonstrate that a similar bistability is also present in a model for large-scale ocean redox chemistry. Via these models, we hence progressively link small-scale observations made in salt marsh sediments, through a more generalized marine sediment system, to the ocean interior. In the final step, we uncover the common underlying cause of the bistability, demonstrating that the bistability is uniquely linked to a restricted set of core reactions that feature in all models examined, of which the precipitation of reduced iron monosulfide (FeS) minerals is the key process responsible for bistability. As FeS formation is common to many anoxic systems, our analysis hence demonstrates how redox bistability emerges as an inherent property of the anoxic marine environment, both in modern times and in the geological past.

Redox Bistability in Salt Marsh Sediments. We start with an analysis of the sediment geochemistry of salt marsh sediments. Recently, it has been observed that stagnant ponds in salt marshes along the Norfolk coast (East Anglia, UK) segregate into two end members that exhibit highly different sediment geochemistry, with pore waters either rich in dissolved ferrous iron or rich in dissolved sulfide (20–22). In the sulfide-rich pond sediment, >70% of the reactive solid-phase iron is reduced and bound to sulfide, while ferrous iron is undetectable in the pore water and dissolved sulfide accumulates to 10 mM (Fig. 2 *A*, *C*, *E*, and *G*). In contrast, in the iron-rich pond sediment, >60% of the solid-phase iron is present in oxidized form and ferrous iron accumulates up to 0.5 mM, with no accumulation of dissolved sulfide (Fig. 2 *B*, *D*, *F*, and *H*) (22). Importantly, these two different redox states can be found in neighboring ponds only a few meters apart (*SI Appendix*, *Materials and Methods*, section 1 and Fig. S1), and this behavior is seen in different salt marsh systems along the ~200-km-long coastline of East Anglia (20, 21). It has been suggested that local differences in iron supply and organic matter input may drive the redox dichotomy (20–22), although it is unclear how the boundary conditions could vary dramatically and systematically over the small distances (<10 m) between ponds. Here, we propose that intrinsic bistability in the coupled cycles of iron and sulfur gives rise to the observed redox dichotomy in the salt marsh pond sediments.

We use the term "bistability" to describe a dynamical system that can be found in either of two stable equilibrium states for identical boundary conditions (Fig. 3*A* provides the classical conceptual representation of such a bistable system). In the case of the salt marsh pond sediments, these two stable states represent pore waters that are either rich in ferrous iron (ferruginous) or rich in dissolved free sulfide (euxinic). The euxinic state is characterized by high dissolved sulfide concentrations and also a higher degree of sulfurization (most iron minerals are in reduced form and bound to sulfide), whereas the ferruginous state is characterized by high concentrations of ferrous iron in the pore water and a lower degree of sulfurization (Fig. 2). If the system starts in an intermediate unstable state, even a small perturbation will direct it toward one of the two stable states (Fig. 3*A*).

To test whether the experimentally observed dichotomy in pond sediment geochemistry (Fig. 2) is an expression of intrinsic bistability in sedimentary Fe and S cycling, we developed a detailed one-dimensional reactive transport model that describes the salt marsh sediment geochemistry in detail, explicitly accounting for different types of iron oxides and organic matter with different reactivities and including all key reactions of the coupled oxygen, carbon, iron, and sulfur cycles (22–24) (*SI Appendix*, *Materials and Methods*, section 2). The model was parameterized using the available data for the East Anglian salt marsh ponds (22). We dynamically ran the sediment model to steady state for different inputs of reactive carbon to the sediment (F_{CH2O}), which is the primary driver of geochemical cycling in sediments. In these simulations, we kept the input of reactive iron oxides to the sediment (F_{FeOOH}) and all other model parameters constant. Note that the F_{CH2O} and F_{FeOOH} fluxes only include those forms of organic carbon and iron oxides that are reactive on early diagenetic timescales (~100 y), and hence they do not incorporate, for example, highly refractory organic carbon or Fe from more poorly reactive iron oxides.

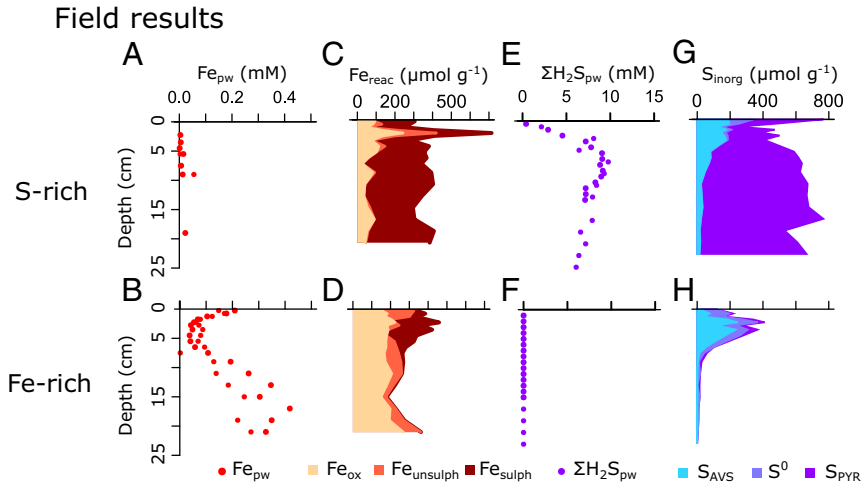

Fig. 2. The redox dichotomy observed in salt marsh sediments. Iron and sulfur speciation data are shown from two nearby ponds in a Norfolk (UK) salt marsh. Panels *A*–*G* show data from the sulfidic pond, while *B*–*H* are data from the ferruginous pond. (*A* and *B*) Pore water dissolved iron (Fe_{pw}). (*C* and *D*) Solid-phase reactive iron (Fe_{reac}) = oxidized iron (Fe_{ox}) + reduced unsulfurized iron ($Fe_{unsulph}$) + reduced sulfurized iron (Fe_{sulph}). (*E* and *F*) Pore water free sulfide (ΣH_2S_{pw} = $[H_2S]$ + $[HS^-]$ + $[S^{2-}]$). (*G* and *H*) Solid-phase inorganic sulfur (S_{inorg}) = acid-volatile sulfide (S_{AVS}) + elemental sulfur (S^0) + pyritic sulfur (S_{PYR}). Data were originally presented in ref. 22.

The model output shows bistable behavior and regime shifts (Fig. 3 *C* and *D*). When running the model for increasing F_{CH2O} values, there is a tipping point past which the system suddenly switches from an Fe-rich state to an S-rich state. When the input of organic carbon is lowered again, the system can be brought back to a ferruginous state, but hysteresis occurs: the forward trajectory differs from the backward trajectory (Fig. 3 *C* and *D*). In particular, upon decreasing F_{CH2O}/F_{FeOOH}, the organic matter input to the system needs to be reduced considerably more before the system shifts back to the Fe-rich state. The two tipping points delineate the bistability zone (F_{CH2O}/F_{FeOOH} ranging between 17.5 and 21; Fig. 3 *C* and *D*), where two steady-state solutions are present for identical boundary conditions (Fig. 3*E*). The model-simulated depth profiles associated with these two alternative stable states are comparable to what is experimentally observed in the salt marsh sediments (Fig. 3*E*).

The observed redox bistability in the model can be explained by a positive feedback between known interactions within the sedimentary Fe and S cycles (Fig. 3*B*). When the F_{CH2O}/F_{FeOOH} ratio is low, the reactive iron oxide input is high enough to suppress sulfide accumulation by limiting sulfate reduction and the reoxidation of sulfide via iron oxides. Under these conditions, the sediment has only a single Fe-rich stable state, characterized by high solid-phase iron oxide (FeOOH) concentrations and ferruginous pore water conditions. If one gradually increases the input of organic matter, the system shows resilience and remains within the Fe-rich state. However, if one increases the input of organic matter sufficiently, the system passes a tipping point beyond which it suddenly shifts from an Fe-rich to a S-rich state, characterized by low FeOOH concentrations and highly sulfidic pore waters (Fig. 3 *C*–*E*). Near the tipping point, the increased organic matter input increases the quantitative importance of sulfate reduction, which generates free sulfide that removes ferrous iron via the formation of solid-phase FeS. At this point, a positive feedback emerges: as FeS precipitates, less ferrous iron gets reoxidized, and so less FeOOH becomes available for dissimilatory iron reduction. This condition then further stimulates sulfate reduction and sulfide production, which further promotes FeS precipitation (Fig. 3*B*). The overall result is a positive feedback, which causes the rapid transition from the Fe-rich to the S-rich state beyond the tipping point.

Because the estimated F_{CH2O} and F_{FeOOH} values for the Norfolk salt marshes are subject to considerable uncertainty, the empirically estimated ratio of organic matter influx over the iron oxide influx (F_{CH2O}/F_{FeOOH}) lies within a broad range from 10 to 34 (*SI Appendix*, *Materials and Methods*, section 1). Still, the median value falls within or near the model-predicted bistability zone (F_{CH2O}/F_{FeOOH} from 17 to 21), and, therefore, bistability provides a plausible explanation for the observed redox dichotomy in the East Anglian salt marsh systems. For example, consider an initial state in which all ponds start in an Fe-rich condition with a low organic matter input. As the marsh develops and vegetation expands with time, the flux of organic matter to the ponds will increase, and so the F_{CH2O}/F_{FeOOH} ratio may approach the tipping point at the right edge of the bistability zone. In this condition, most ponds remain Fe dominated, but some ponds may receive a small additional input of organic matter for a short while, upon which they pass the tipping point and shift to an S-dominated state. Due to the hysteresis effect, these ponds will not go back to an Fe-dominated state when the temporary additional input of organic matter ceases but will tend to remain in the S-dominated state. As a result, one obtains a marsh where all ponds receive the same input of organic matter but show a redox dichotomy; some ponds will still have the Fe-rich state, while others have irreversibly switched to an S-rich state (20–22). The S-rich ponds can only switch back to an Fe-rich state when the organic matter input to the ponds decreases enough to pass the left tipping point of the bistability zone. The important consequence is that the observed redox dichotomy in the salt marsh sediments may not reflect present differences in boundary conditions but may instead be path dependent.

Generalization to Marine Sediments. The phenomenon of Fe/S bistability is not restricted to salt marsh sediments. We demonstrate this in a generalized reactive transport model of a marine sediment (*SI Appendix*, *Materials and Methods*, section 3). The model includes a set of transport and reaction processes common to models that have been previously used to describe early diagenesis in a variety of marine sediment environments (24–28). The model is run over a broad range of systematically varied parameter values, and these model simulations provide insight into the prevalence of Fe/S bistability (*SI Appendix*, Figs. S2 and S3). One crucial constraint is that sediments receive a sufficient input of organic carbon and iron oxides so that they become anoxic, with dissimilatory iron and sulfate reduction becoming competing mineralization pathways. Slope and deep-sea sediments in the modern ocean are generally oxic and dominated by aerobic

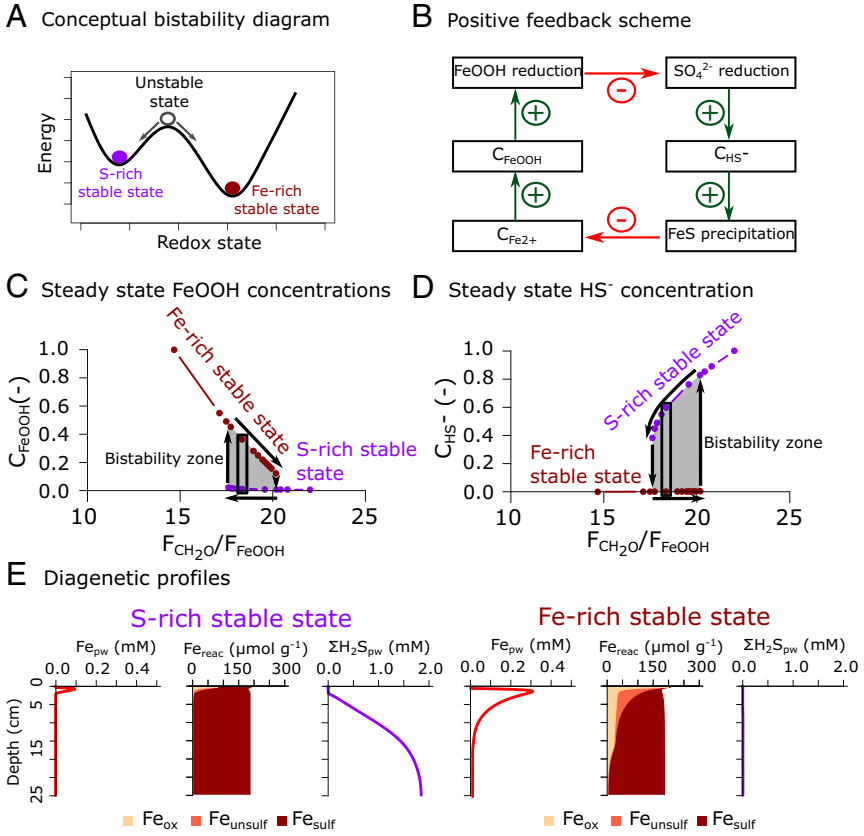

Fig. 3. (*A*) A conceptual illustration of bistability in iron–sulfur geochemistry. For a certain set of boundary conditions (e.g., the flux of organic matter and iron oxides), the dominant redox state of an anoxic system can be either sulfide rich or iron rich. See the article text for details. (*B*) The positive feedback scheme that generates bistability in the geochemistry of anoxic systems. See the article text for details. (*C–E*) The model results for the reactive transport model of salt marsh sediments (*SI Appendix, Materials and Methods*, section 2). (*C*) The steady-state concentration of reactive iron oxide (C_{FeOOH}) versus the ratio of organic matter influx (F_{CH2O}) and iron oxide influx (F_{FeOOH}). (*D*) The steady-state concentration of dissolved sulfide (C_{HS-}) versus the ratio of organic matter influx and iron oxide influx. The *y* axis in *C* and *D* are normalized against the maximum concentration in the plot for clarity. Each point represents the results from a single steady-state model simulation. The bistability zone (gray zone) occurs when two divergent steady states are present for identical input parameters. The purple dots indicate the S-rich state; the red dots indicate the Fe-rich state. The arrows indicate the direction of the hysteresis loop. The black box indicates the steady-state model simulation for which the diagenetic profiles are shown in *E*. (*E*) The diagenetic profiles for the S-rich and Fe-rich stable states.

respiration (29) and hence are not prone to regime shifts. In contrast, the Fe/S bistability may be an inherent feature of many modern coastal and shelf sediments and generally occurs around a value of F_{CH2O}/F_{FeOOH} ~15 (*SI Appendix*, Fig. S3). A compilation of the F_{CH2O}/F_{FeOOH} ratios for several coastal and shelf sediments shows that these sediments indeed fall close to or within the model-predicted bistability ranges (*SI Appendix*, Table S10). We find that the width of the bistability zone becomes smaller for higher rates of sediment mixing by marine infauna, which suggests that Fe/S bistability could have been more prevalent in shallow seafloor environments without benthic fauna, as was the case before the Phanerozoic. Similarly, the hysteresis decreases for increasing sedimentation rates, as higher sedimentation will increase the burial of FeS minerals, thereby promoting the S-rich state. A wide bistability zone is generally present at sedimentation rates below ~0.2 cm/yr^{-1} (*SI Appendix*, Fig. S3). This transport regime applies to most of the present-day coastal seafloor, apart from regions with high accumulation like the deltaic mobile muds of the Amazon delta (30).

While coastal and shelf sediments appear susceptible to bistability, the existence of hysteresis may explain why the phenomenon has not previously been identified in field studies. Sites residing within the middle of the bistability zone would tend to be "locked" in an Fe-rich or S-rich state, and revisiting the same site multiple times would yield the same observed state. Only when a sediment system is poised at the edge of the bistability zone and external boundary conditions (like organic matter delivery) show suitable spatial or temporal variation will one observe both Fe-rich and S-rich states within a given area. This particular situation is likely not often encountered in the field but could be the case in the East Anglian salt marsh systems, as discussed above. Another potential location is the Arvadi Springs, where S-rich and Fe-rich sediments are found to coexist on spatial scales of <1 m, without apparent differences in organic matter input (31).

The bistability in Fe and S cycling has important ramifications for studies on modern marine sediment geochemistry as well as for the interpretation of the geologic record. Firstly, as a consequence of the existence of hysteresis, the particular geochemical state observed in a sediment may depend on the history of the system. A second ramification is that one-to-one mapping between observed concentrations in the sediment and inferred input fluxes breaks down within the bistability interval, as a system can be either ferruginous or euxinic for the same F_{CH2O}/F_{FeOOH} ratio. Therefore, in ancient deposits, one cannot make strong inferences about the influx of organic matter solely based on sedimentary redox proxies. Sediments with ferruginous and euxinic pore waters may underly water columns with nearly the same productivity.

Extension to Ocean Geochemical Dynamics. To explore whether the Fe/S bistability can also be present in natural systems other than sediments, we equipped a three-box ocean model (16, 32) with a set of biogeochemical reactions describing the cycling of carbon, iron, and sulfur (*SI Appendix*, *Materials and Methods*, section 4 and Fig. S4). The model was parameterized to represent the present-day ocean in terms of large-scale circulation, particle sinking fluxes, and export production. We dynamically ran this ocean model to steady state for different values of ocean export production (J_{CH2O}; this forms the counterpart of F_{CH2O} in the sediment model) and O_2 partial pressures in the atmosphere, keeping the weathering fluxes of reactive iron oxides and sulfate to the ocean constant. While the spatial scales and transport mechanisms are very different compared to sediments, the ocean model consistently exhibited comparable redox bistability (*SI Appendix*, Fig. S5). Furthermore, for increasing (and then decreasing) J_{CH2O} values, the model output traces out a similar hysteresis loop (Fig. 4*A*). Low values of J_{CH2O} lead to ferruginous conditions, which can switch to euxinic conditions when J_{CH2O} is increased past a tipping point. Moreover, we find that there is a coherent scaling in the location of the bistable region as a function of atmospheric pO_2 (Fig. 4). For example, for an atmospheric O_2 concentration of 0.1 present atmospheric level (PAL), the bistability zone emerges between 45 and 47% of present-day oceanic export production, while for 0.01 PAL, the bistability zone arises at lower productivity, between 5 and 6% of present-day oceanic export production (Fig. 4 *A* and *B*).

Our ocean box model predicts a much narrower bistability zone (gray zone in Fig. 4*A*; thin black wedge in Fig. 4*B*) than exhibited by a sediment system. In the sediment, the zone of hysteresis becomes smaller when vertical transport (sedimentation) increases (*SI Appendix*, Fig. S3). In the oceanic water column, the residence time of sinking particles is much shorter (~10 to 100 d) compared to shelf sediments (>50 y). This strong vertical transport partly explains why, in an oceanic setting, the Fe/S redox bistability falls within a significantly more restricted region of the parameter space. Importantly, the narrow bistability zone implies that oceanic systems are more prone to observable redox shifts than sedimentary systems. Small changes in oceanic export production, on the order of just a few percent, may shift the deep ocean back and forth across the narrow bistability zone, thus inducing repeated switches between ferruginous and euxinic states.

The occurrence of oceanic regime shifts crucially depends on the export production at any given partial pressure of atmospheric oxygen (Fig. 4*B*). Interestingly, recent estimates for productivity and atmospheric oxygen during the Proterozoic (33, 34) suggest that the ocean interior could have been within or near the bistable region for much of Proterozoic time (Fig. 4*B*), which may explain the alternation between ferruginous and euxinic states observed in the rock record. Further model analysis shows that the key parameters determining the location and width of the bistability zone are the strength of ocean circulation (mixing) and the rate at which particles sink in the ocean; the bistability zone becomes larger with increasing strength of ocean circulation and decreasing particle sinking fluxes (*SI Appendix*, Fig. S5). These parameters are difficult to constrain through time but will have varied throughout Earth's history as a consequence of plate tectonics and biological evolution (see, e.g., refs. 35–37). Interestingly, at atmospheric oxygen partial pressures equivalent to 0.1 PAL, oceanic sulfate abundance has only a negligible influence on the location and width of the bistable region. The bistability zone appears at the same level of export production for oceanic sulfate concentrations that range from a few micromolar to millimolar levels (*SI Appendix*, Fig. S6). This implies that transitions from ferruginous to euxinic conditions need not be linked solely to variations in sulfate runoff from terrestrial weathering. However, at lower atmospheric oxygen levels, the bistability zone disappears for sulfate levels of a few micromolars, which could suggest that the Fe/S bistability was less important in the Archean oceans (38, 39).

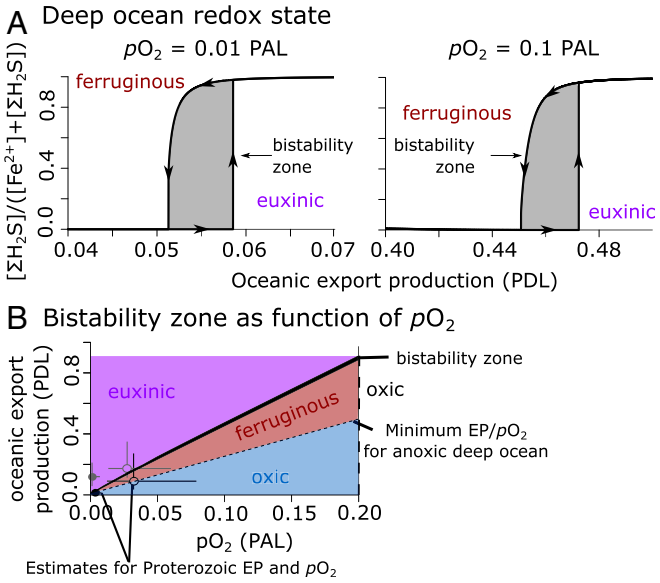

Fig. 4. Bistability in the ocean interior. (*A*) A sensitivity analysis of a three-box ocean model. The steady-state model results are displayed for an atmospheric O_2 concentration of 0.01 PAL and 0.1 PAL. A bistability zone (gray zone) appears between 0.05 and 0.06 present-day level (PDL) and 0.45 and 0.47 PDL of export production, respectively. The arrows indicate the direction of the hysteresis loop. (*B*) The location of the bistability zone (thin black wedge) for different pO_2 concentrations. The dashed vertical line on the right indicates the pO_2 for which the deep ocean box becomes oxic. The dashed diagonal line shows the minimum ratio of export production (EP) over pO_2 consistent with an anoxic deep ocean as derived from a three-dimensional ocean-based model (cGEnIE) (15). The gray symbols show the median (circles) and 90% credible intervals (error bars) on export production estimated from an intermediate-complexity ocean biogeochemistry model (33). The results are shown for both low-O_2 (closed) and high-O_2 (open) scenarios. The black symbols show the median (circles) and 90% credible intervals (error bars) on export production based on the oxygen isotope composition of evaporitic sulfate minerals (34), assuming 20% of the gross primary production is exported from the photic zone (48). The results are shown for both low-O_2 (closed) and high-O_2 (open) scenarios.

Iron Sulfide Formation Drives Fe/S Bistability. Finally, to illustrate how we can confidently make the stretch from modern observations in salt marsh sediments to potential Precambrian ocean states and transitions, we need to expose the core mechanism that causes redox bistability. To this end, we reduced the sediment and ocean system to its barest biogeochemical essentials and reformulated transport as a zero dimensional (0D) chemostat-type description, while the reaction set was progressively simplified to eventually only retain those reactions that generate the Fe/S bistability (*SI Appendix*, *Materials and Methods*, section 5). These key interactions include the following: 1) the oxidation of organic matter by dissimilatory iron and sulfate reduction, 2) the reoxidation of Fe^{2+} and H_2S by oxygen, and 3) the precipitation of FeS. These reactions are common to all ocean and sediment models examined above. After suitable reformulation, we were able to condense the 0D chemostat model into a single ordinary differential equation that describes the dynamic behavior of the reactive iron oxide concentration (C_{FeOOH}), supplemented with algebraic equations for the concentrations of Fe^{2+} and H_2S.

Overall, this highly simplified and abstract model enables classical linear stability analysis (Fig. 5) and generates a very

similar dynamical response as the more complex models analyzed above. For low F_{CH2O} inputs, there is only one single ferruginous stable state (high C_{FeOOH}; low C_{HS-}), while at higher F_{CH2O} inputs, there is a single euxinic state (low C_{FeOOH}; high C_{HS-}). In between, there is a bistability zone that shows hysteresis induced by two saddle-point bifurcations, which is the archetypal fingerprint of a dynamical system exhibiting regime shifts (Fig. 5 *A* and *B*). Most importantly, this abstract model demonstrates that FeS formation is the key reaction responsible for the positive feedback that generates the bistability (*SI Appendix*, *Materials and Methods*, section 5 and Figs. S7 and S8). In a reaction system where FeS precipitation is hypothetically inhibited, there is only a single, Fe-rich stable state (Fig. 5*C*). However, when FeS formation is kinetically fast, as is the case in natural environments, the reaction system exhibits two alternative stable states (Fig. 5*D*): the Fe-rich (C_{FeOOH} ~6, Fig. 5*D*) and S-rich (C_{FeOOH} ~0, Fig. 5*D*) states described above. Our analysis thus demonstrates that the Fe/S bistability is uniquely associated with the occurrence of FeS formation, and its occurrence is not fundamentally influenced by the inclusion of other Fe and S reactions in the reaction set. These other Fe and S reactions do not determine the presence of the bistability but only modulate the shape of the stability zone. This also explains why the Fe/S bistability is generically present in all ocean and sediment models examined.

Conclusions and Perspectives

Our model analysis supports the existence of redox bistability in marine sediments and explains the redox dichotomy observed in modern marine aquatic sediments (20–22). At the same time, it provides a parsimonious explanation both for shifts in the ocean redox state that occurred from the late Archean to the early Phanerozoic (9, 17) as well as the short-term redox oscillations observed in the mid-Cretaceous (11). However, the dependence of ocean redox shifts on export productivity does not obviate the potential impact of changes in sulfur and iron fluxes on the nature of ocean anoxia. Essentially, the interplay between export productivity and the fluxes of sulfur and iron will determine whether a system shifts between ferruginous and euxinic states. If the sulfate flux to the ocean is too low, sulfide production cannot completely remove all ferrous iron from solution, and the ocean interior will not shift to an euxinic state (19). Conversely, if the sulfate flux is high enough to generate euxinia but productivity is too low, the ocean will also not shift to an euxinic state.

Because nutrient availability is strongly dependent on the redox state, the existence of redox bistability has potentially profound implications for the causes and consequences of marine evolutionary innovations and ecological transitions. For instance, phosphate limitation could have been maintained in a ferruginous ocean via scavenging by iron oxides near the ocean surface or precipitation of ferrous phosphate minerals (12, 40, 41), keeping primary productivity low enough to stay below the bistability threshold. In contrast, any transition induced to euxinic conditions could lead to the occurrence of iron or other trace element limitation (11, 13), eroding the stability of the euxinic state and driving the system back to ferruginous conditions. This could in large part explain the existence of predominantly ferruginous redox conditions in the ocean interior throughout much of the Precambrian, as implied by the rock record (7, 19). The potential for such an interplay and feedback between the ocean redox state, nutrient availability, and marine productivity, and, ultimately, with the evolution of marine life, hints at a hitherto-underappreciated complexity in the dynamics of the Earth system. As such, our work has implications for understanding the causes of past transitions in ocean biogeochemistry and their consequences for the biosphere.

The fact that bistability and hysteresis emerge within a simplified ocean model as well as different reactive transport models of sediment biogeochemistry suggests that it is deeply rooted within anoxic systems, and, hence, the phenomenon should also

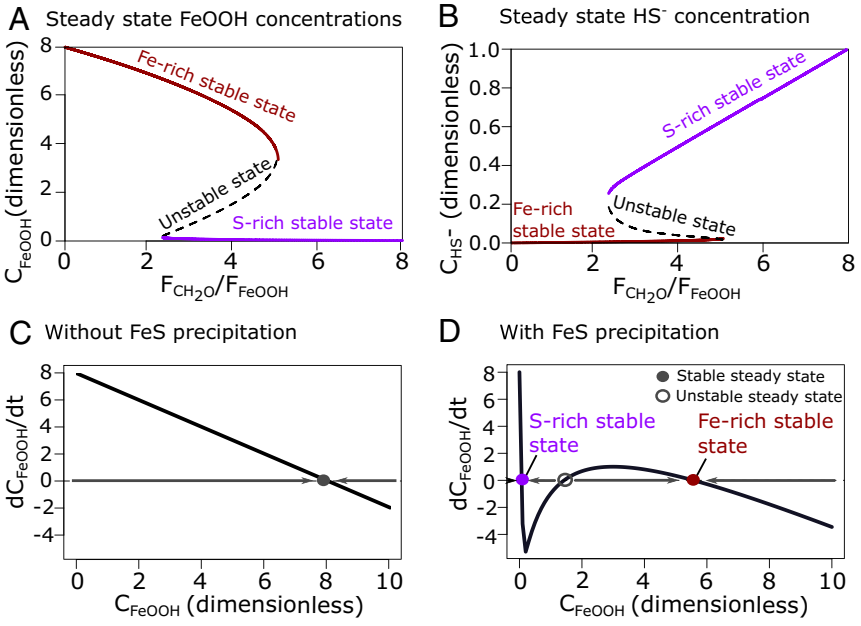

Fig. 5. A mathematical analysis of bistability based on an abstract 0D model that includes reactions common to all complex ocean and sediment models previously examined (*SI Appendix*, *Materials and Methods*, section 5). (*A*) The steady-state FeOOH concentrations (C_{FeOOH}) versus the ratio of organic matter influx (F_{CH2O}) and iron (oxyhydr)oxide influx (F_{FeOOH}). (*B*) The steady-state concentration of dissolved sulfide (C_{HS-}) versus the ratio of organic matter influx and iron (oxyhydr)oxide influx. (*C*) A phase plot showing the relation between the rate of change of oxidized iron (dC_{FeOOH}/dt) and the concentration of oxidized iron (C_{FeOOH}) when FeS precipitation is negligible compared to reoxidation of ferrous iron and dissolved sulfide. The system shows a single stable state. (*D*) A similar phase plot when FeS precipitation is much faster than reoxidation of ferrous iron and dissolved sulfide. The system shows two separate stable states and one unstable state. *C* and *D* show results for F_{CH2O}/F_{FeOOH} ratio of 4. Concentrations in *C* and *D* are in dimensionless form.

emerge in more complex models (e.g., ref. 11). Still, one should be aware of the limitations of the ocean and sediment models employed here. For instance, our sediment models assume that iron oxide minerals only consist of one or two fractions with different reactivities toward sulfide. Accounting for more complex iron mineralogy (e.g., by including green rust, likely an important mineral in Precambrian environments (31)) will likely not prevent the occurrence of bistability but could affect the location or width of the bistability zone. Likewise, our ocean model analysis is based on steady state, so we cannot make any inferences about the frequency of redox shifts or whether these match periodicities observed in Earth's rock record. Also, the three-box ocean model employed here does not capture any spatial variation in redox conditions, and as a result, we cannot assess whether increasing spatial resolution and heterogeneity of the ocean environment may lead to loss of redox bistability. Therefore, an important next step is to investigate the phenomenon in a dynamical and spatially resolved Earth system model and conduct both transient and steady-state simulations. This will allow for making explicit comparisons with the geological record and its attendant redox proxies.

Materials and Methods

All computer code associated with the models described below is available from https://github.com/sevdevel/PNAS2020. All data presented in Fig. 2 is available in the *SI Appendix*.

Reactive Transport Sediments Models of Fe and S Cycling in Marine Sediments. To test the hypothesis that the redox dichotomy found in Blakeney salt marsh is caused by redox bistability, we developed a detailed one-dimensional reactive transport model for marine sediments, which includes all key reactions of the coupled oxygen, carbon, iron, and sulfur cycles. The model is described in detail in *SI Appendix, Materials and Methods*, section 2. In short, organic matter mineralization is modeled using a 14-component multi-G model, following ref. 23. Each organic matter fraction ("G") can be degraded by oxygen, iron oxide, or sulfate or via methanogenesis, following the thermodynamic redox sequence. Iron oxide reduction and sulfate reduction are allowed to overlap, as at circumneutral pH, the thermodynamic energy gain of both reactions is similar (42). Iron oxides are modeled as two separated fractions with different reactivities toward sulfide. The reduction of iron oxide produces ferrous iron, which can adsorb on solid-phase particles, react with dissolved sulfide to form iron monosulfide, and be reoxidized with oxygen. Sulfide generated by sulfate reduction can be reoxidized after reaction with iron oxide or oxygen, precipitate as iron monosulfide, or react with iron monosulfide to form pyrite. When all electron acceptors are depleted, organic matter is degraded via fermentation with the production of methane. The transport is governed by molecular diffusion, sedimentation, and biomixing.

To assess the sensitivity of the redox bistability, we generalized and simplified the reactive-transport model (described in detail in *SI Appendix, Materials and Methods*, section 3) to make subsequent runs more computationally efficient. This simplified model is used to illustrate the sensitivity of key environmental parameters (biomixing intensity, iron oxide flux, and sedimentation velocity). We omitted methanogenesis, combined all organic matter fractions ("G's") into one, combined both iron oxide fractions into one, and omitted pyrite precipitation.

Three-Box Ocean Geochemistry Model. To investigate whether redox bistability also shows up in ocean redox models, we developed a three-box Harvardton–Bear–type model (see, e.g., ref. 16). The model is detailed in *SI Appendix, Materials and Methods*, section 4. Briefly, we implemented the same set of reactions as for the simplified reactive transport model of a marine sediment but included methanogenesis, replaced iron monosulfide precipitation with pyrite precipitation, and included gypsum formation. This model includes a highly simplified description of ocean dynamics but should serve as an inspiration for future studies with spatially explicit ocean models.

An Idealized 0D Chemostat Model of Sedimentary Fe and S Cycling. To find the underlying cause of this bistability, we performed an extensive mathematical analysis of the core reactions of the coupled C–Fe–S cycles (described in detail in *SI Appendix, Materials and Methods*, section 5). To be able to conduct this mathematical analysis, several simplifications had to made to arrive at an idealized description of Fe and S cycling in anoxic environments. Firstly, the model domain was defined as one-box; aerobic respiration, iron monosulfide dissolution, and sulfide-mediated iron reduction were omitted. An analysis with the simplified one-dimensional reactive transport model indicated that these reactions do not significantly affect model outcomes (*SI Appendix*, Fig. S2). Secondly, as we target environments that are dominated by iron or sulfate reduction, we do not consider fully oxic or methanic environments, so we can assume that only a low level of oxygen is present that can oxidize reduced ferrous iron and dissolved sulfide. Additionally, we assume sulfate is always high enough to suppress methanogenesis. Note that these simplifications are only made to derive a mathematical expression of redox bistability.

Data Availability. Model source codes and simulation files have been deposited in GitHub (https://github.com/sevdevel/PNAS2020).

ACKNOWLEDGMENTS. The research leading to these results was financially supported by the Belgian American Educational Foundation and the National Aeronautics and Space Administration (NASA) Postdoctoral Program (postdoctoral Fellowship to S.J.v.D.V.). F.J.R.M. was supported by the Research Foundation Flanders via Fonds Wetenschappelijk Onderzoek Grant G038819N and the Netherlands Organization for Scientific Research (VICI Grant 016.VICI.170.072). A.R. acknowledges support from the NSF under Grant No. 1736771 and from the Heising–Simons Foundation. C.T.R. acknowledges support from the NASA Astrobiology Institute and the NASA Nexus for Exoplanet System Science.

1. R. E. Keeling, A. Körtzinger, N. Gruber, Ocean deoxygenation in a warming world. *Annu. Rev. Mar. Sci.* **2**, 199–229 (2010).
2. C. T. Scott *et al.*, Late Archean euxinic conditions before the rise of atmospheric oxygen. *Geology* **39**, 119–122 (2011).
3. R. Guilbaud, S. W. Poulton, N. J. Butterfield, M. Zhu, G. A. Shields-zhou, A global transition to ferruginous conditions in the early Neoproterozoic oceans. *Nat. Geosci.* **8**, 466–470 (2015).
4. N. J. Planavsky *et al.*, Evidence for episodic oxygenation in a weakly redox-buffered deep mid-Proterozoic ocean. *Chem. Geol.* **483**, 581–594 (2018).
5. B. Kendall *et al.*, Pervasive oxygenation along late Archaean ocean margins. *Nat. Geosci.* **3**, 647–652 (2010).
6. E. A. Sperling *et al.*, Redox heterogeneity of subsurface waters in the Mesoproterozoic ocean. *Geobiology* **12**, 373–386 (2014).
7. N. J. Planavsky *et al.*, Widespread iron-rich conditions in the mid-Proterozoic ocean. *Nature* **477**, 448–451 (2011).
8. E. A. Sperling, G. P. Halverson, A. H. Knoll, F. A. Macdonald, D. T. Johnston, A basin redox transect at the dawn of animal life. *Earth Planet. Sci. Lett.* **371–372**, 143–155 (2013).
9. J. F. Emmings *et al.*, A Mississippian black shale record of redox oscillation in the Craven Basin, UK. *Palaeogeogr. Palaeoclimatol. Palaeoecol.* **538**, 109423 (2020).
10. S. W. Poulton *et al.*, A continental-weathering control on orbitally driven redox-nutrient cycling during Cretaceous Oceanic Anoxic Event 2. *Geology* **43**, 963–966 (2015).
11. K. Wallmann *et al.*, Periodic changes in the Cretaceous ocean and climate caused by marine redox see-saw. *Nat. Geosci.* **12**, 456–461 (2019).
12. C. T. Reinhard *et al.*, Evolution of the global phosphorus cycle. *Nature* **541**, 386–389 (2017).
13. C. T. Reinhard *et al.*, Proterozoic ocean redox and biogeochemical stasis. *Proc. Natl. Acad. Sci. U.S.A.* **110**, 5357–5362 (2013).
14. R. A. Boyle *et al.*, Nitrogen cycle feedbacks as a control on euxinia in the mid-Proterozoic ocean. *Nat. Commun.* **4**, 1533 (2013).
15. T. M. Lenton, S. J. Daines, Biogeochemical transformations in the history of the Ocean. *Annu. Rev. Mar. Sci.* **9**, 31–58 (2017).
16. D. E. Canfield, A new model for Proterozoic ocean chemistry. *Nature* **396**, 450–453 (1998).
17. R. Raiswell, D. E. Canfield, The iron biogeochemical cycle past and present. *Geochem. Perspect.* **1**, 1–220 (2012).
18. D. T. Johnston *et al.*, An emerging picture of neoproterozoic ocean chemistry: Insights from the chuar group, grand Canyon, USA. *Earth Planet. Sci. Lett.* **290**, 64–73 (2010).
19. S. W. Poulton, D. E. Canfield, Ferruginous conditions: A dominant feature of the Ocean through Earth's history. *Elements* **7**, 107–112 (2011).
20. G. Antler, J. V. Mills, A. Huthings, K. Redeker, A. V. Turchyn, The sedimentary carbon-sulfur-iron interplay–A lesson from East Anglian salt marsh sediments. *Front. Earth Sci.* **7**, 140 (2019).
21. A. M. Hutchings *et al.*, Creek dynamics determine pond subsurface geochemical heterogeneity in East Anglian (UK) salt marshes. *Front. Earth Sci.* **7**, 41 (2019).
22. S. van de Velde *et al.*, Burrowing fauna mediate alternative stable states in the redox cycling of salt marsh sediments. *Geochim. Cosmochim. Acta* **276**, 31–49 (2020).
23. A. W. Dale *et al.*, A revised global estimate of dissolved iron fluxes from marine sediments. *Global Biogeochem. Cycles* **29**, 1–17 (2015).
24. P. Berg, S. Rysgaard, B. Thamdrup, Dynamic modeling of early diagenesis and nutrient cycling. A case study in an Artic Marine sediment. *Am. J. Sci.* **303**, 905–955 (2003).
25. Y. Wang, P. Van Cappellen, A multicomponent reactive transport model of early diagenesis: Application to redox cycling in coastal marine sediments. *Geochim. Cosmochim. Acta* **60**, 2993–3014 (1996).

26. F. J. R. Meysman, J. J. Middelburg, P. M. J. Herman, C. H. R. Heip, Reactive transport in surface sediments. II. Media: An object-oriented problem-solving environment for early diagenesis. *Comput. Geosci.* **29**, 301–318 (2003).
27. S. van de Velde, F. J. R. Meysman, The influence of bioturbation on iron and sulphur cycling in marine sediments: A model analysis. *Aquat. Geochem.* **22**, 469–504 (2016).
28. K. Soetaert, P. M. J. Herman, J. J. Middelburg, A model of early diagenetic processes from the shelf to abyssal depths. *Geochim. Cosmochim. Acta* **60**, 1019–1040 (1996).
29. D. Steven *et al*., Presence of oxygen and aerobic communities from sea floor to basement in deep-sea sediments. *Nat. Geosci.* **8**, 299–304 (2015).
30. R. C. Aller, "8.11 - Sedimentary diagenesis, depositional environments, and benthic fluxes" in *Treatise on Geochemistry*, H. D. Holland, K. K. Turekian, Eds. (Elsevier Ltd., ed. 2, 2014), pp. 293–334.
31. E. Koeksoy *et al*., A case study for late Archean and Proterozoic biogeochemical iron- and sulphur cycling in a modern habitat-the Arvadi Spring. *Geobiology* **16**, 353–368 (2018).
32. B. P. Boudreau, J. J. Middelburg, A. F. Hofmann, F. J. R. Meysman, Ongoing transients in carbonate compensation. *Global Biogeochem. Cycles* **24**, 1–13 (2010).
33. K. Ozaki, C. T. Reinhard, E. Tajika, A sluggish mid-Proterozoic biosphere and its effect on Earth's redox balance. *Geobiology* **17**, 3–11 (2019).
34. P. W. Crockford *et al*., Triple oxygen isotope evidence for limited mid-Proterozoic primary productivity. *Nature* **559**, 613–616 (2018).
35. Y. Donnadieu, E. Pucéat, M. Moiroud, F. Guillocheau, J. F. Deconinck, A better-ventilated ocean triggered by Late Cretaceous changes in continental configuration. *Nat. Commun.* **7**, 10316 (2016).
36. G. A. Logan, J. M. Hayes, G. B. Hieshima, R. E. Summons, Terminal Proterozoic reorganization of biogeochemical cycles. *Nature* **376**, 53–56 (1995).
37. K. M. Meyer, A. Ridgwell, J. L. Payne, The influence of the biological pump on ocean chemistry: Implications for long-term trends in marine redox chemistry, the global carbon cycle, and marine animal ecosystems. *Geobiology* **14**, 207–219 (2016).
38. S. A. Crowe *et al*., Sulfate was a trace constituent of Archean seawater. *Science* **346**, 735–739 (2014).
39. M. Fakhraee, O. Hancisse, D. E. Canfield, S. A. Crowe, S. Katsev, Proterozoic seawater sulfate scarcity and the evolution of ocean–atmosphere chemistry. *Nat. Geosci.* **12**, 375–380 (2019).
40. R. Guilbaud *et al*., Phosphorus-limited conditions in the early Neoproterozoic ocean maintained low levels of atmospheric oxygen. *Nat. Geosci.* **13**, 296–301 (2020).
41. L. A. Derry, Causes and consequences of mid-Proterozoic anoxia. *Geophys. Res. Lett.* **42**, 8538–8546 (2015).
42. D. Postma, R. Jakobsen, Redox zonation: Equilibrium constraints on the Fe(III)/SO4-reduction interface. *Geochim. Cosmochim. Acta* **60**, 3169–3175 (1996).
43. C. T. Reinhard, S. L. Olson, E. W. Schwieterman, T. W. Lyons, False negatives for remote life detection on Ocean-bearing planets: Lessons from the early Earth. *Astrobiology* **17**, 287–297 (2017).
44. N. J. Planavsky *et al*., Evidence for oxygenic photosynthesis half a billion years before the Great Oxidation Event. *Nat. Geosci.* **7**, 283–286 (2014).
45. C. M. Ostrander *et al*., Fully oxygenated water columns over continental shelves before the Great Oxidation Event. *Nat. Geosci.* **12**, 186–191 (2019).
46. S. L. Olson, L. R. Kump, J. F. Kasting, Quantifying the areal extent and dissolved oxygen concentrations of Archean oxygen oases. *Chem. Geol.* **362**, 35–43 (2013).
47. C. T. Reinhard, R. Raiswell, C. T. Scott, A. D. Anbar, T. W. Lyons, A late archean Sulfidic Sea stimulated by early oxidative weathering of the Continents. *Science* **326**, 713–716 (2009).
48. J. P. Dunne, J. L. Sarmiento, A. Gnanadesikan, A synthesis of global particle export from the surface ocean and cycling through the ocean interior and on the seafloor. *Global Biogeochem. Cycles* **21**, 1–16 (2007).